High-Accuracy Online Calibration Scheme for Large-Scale Integrated Photonic Interferometric Measurements

Yi Zhang, Kun Wang, Qichang An, Yinlei Hao, Haoran Meng, and Xinyue Liu

***Abstract*—High-accuracy interferometric measurement is crucial for integrated photonic interferometric imaging. In this paper, we propose an online calibration approach for large-scale integrated photonic beam combination that can realize high-accuracy measurement. By leveraging a simple four-step switching condition and the optical path differences between interferometric beams, the instrumental characteristics of the beam combiner, including the transmittances, visibilities, and phase relations, could be calibrated accurately. Compared to the conventional approach, the calibration procedure and estimation method are greatly simplified in our proposed scheme. The effectiveness of the proposed approach is validated using a photonic integrated circuit with two interferometric channels. The calibration results show that the differences between the phase relations are less than 1.41% between the proposed and conventional approaches. The proposed scheme shows significant advantages in optical synthetic aperture imaging systems using photonic integrated circuits especially for applications in harsh environments.**

***Index Terms*—Instrumental visibility, online calibration, photonic integrated beam combination, V2PM.**

I. Introduction

PHOTONIC integrated beam combination is a transformational technique for optical aperture synthesis interferometric imaging in which photonic integrated circuits (PICs) are used, rather than bulk optical components, to realize large-scale interferometric beam combination [1]–[3]. This method has the potential to enhance optical aperture synthesis for real-time imaging and multi-spectral imaging, among others [4]. The basic concept of photonic integrated beam combination was initially proposed and implemented for astronomical optical long baseline interferometry [5]. Since then, it has been successfully implemented in telescopes, such as VINCI/Very Large Telescope Interferometer (2 telescopes) [6], IONIC/Infrared Optical Telescope Array (3 telescopes) [7], and GRAVITY/Very Large Telescope Interferometer (4 telescopes) [8]. Furthermore, Segmented Planar Imaging Detector for Electro-optical Reconnaissance (SPIDER) implements the large-scale PICs for the multi-channel and multi-spectral interferometric beam combination, based on which the solutions are proposed for the snapshot optical aperture synthesis imager with the advantages of ultra-thinness and ultra-lightness [9]–[13]. With recent advances in integrated photonics, integrated photonic interferometric imaging has attracted significant attention [14]–[18].

Based on the van Cittert-Zernike theorem [19], aperture synthesis imaging can be realized using photonic integrated interferometer arrays with the "pairwise static ABCD" scheme for multi-channel interferometric measurements [20]. However, the machining and assembly errors of PICs can affect the accuracy of interferometric imaging [21]. Moreover, characteristics of light propagation in PIC are sensitive to external environmental factors, such as temperature and vibration, that affect the optical waveguide length, the refractive index and the internal stress cause a change in the phase of the guided light. These sensitives have a negative impact on the interferometric visibility measurement, eventually distorting the reconstructed images [22]. Thus, efficient online calibration is crucial for assuring high-accuracy interferometric imaging.

For the four-channel photonic integrated beam combiner in Very Large Telescope Interferometer, Bensity *et al.* proposed a characterization approach based on the visibility to pixel matrix (V2PM) estimator [23]. V2PM characterizes the instrumental behavior of beam combiners by photometric measurements as well as wide-range temporal modulation of OPDs and the envelope fitting of interferometric patterns [24]. This characterization approach is used in ground-based long-baseline interferometers, where subsystems such as beam-train systems, delay lined, beam combining facilities, and interferometer control systems are arranged in vibration-isolated and thermally regulated laboratories to maintain stable operating conditions [25]. The validity period of the obtained calibration results is generally long. However, the validity period is short for moving platforms with limited space in harsh environments, such as space-borne and air-borne applications. This requires frequent recalibrations via complicated calibration and estimation methods, affecting the adaptability of V2PM to rapid environmental changes. Thus, it is

Manuscript received December 7, 2021; revised March 30, 2022; accepted April 7, 2022. Date of publication April 12, 2022; date of current version May 6, 2022. This work was supported by the Youth Innovation Promotion Association CAS under Grant 2020221. *(Corresponding author: Qichang An.)*

Yi Zhang and Kun Wang are with the Changchun Institute of Optics, Fine Mechanics and Physics, Chinese Academy of Sciences, Changchun 130033, China, and also with the University of Chinese Academy of Sciences, Beijing 100049, China (e-mail: zhangyi164@mails.ucas.ac.cn; jlwangkun2@163.com).

Qichang An, Haoran Meng, and Xinyue Liu are with the Changchun Institute of Optics, Fine Mechanics and Physics, Chinese Academy of Sciences, Changchun 130033, China (e-mail: 13943083982@163.com; ranokok@gmail.com; liuxinyue@ciomp.ac.cn).

Yinlei Hao is with the Zhejiang University, Hangzhou 310027, China (e-mail: haoyinlei@zju.edu.cn).

Digital Object Identifier 10.1109/JPHOT.2022.3166529

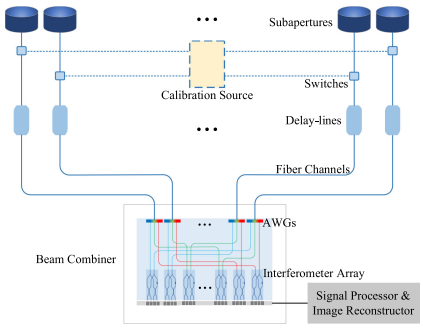

Fig. 1. Schematic layout of the photonic integrated interferometric imaging system.

extremely difficult to apply above scheme in online calibration, especially for large-scale beam combination tasks, such as in SPIDER.

In this study, we generalize the characterization approach to derive a modified representation of the V2PM estimator, which simplifies the calibration procedure and estimation method significantly. Based on the modified V2PM, we propose an approach through a simple four-step setting of the switching conditions and OPDs between the interferometric channels, and we validated its effectiveness for high-accuracy interferometric measurement through experimental comparisons. In general, interferometric imaging systems are equipped with optical delay lines for fringe tracking to improve imaging performance [26]. Thus, components such as optical path and optical delay lines can be reused to reduce the system load. The instrumental matrix can be calibrated by simply installing the calibration source, and the interferometric imaging system can switch between the imaging and calibration modes at any time by optical switching, based on changes in the external environment. Therefore, the proposed approach can realize online high-accuracy calibration for large-scale photonic integrated interferometric measurements.

The remainder of this paper is arranged as follows. Section II introduces the derivation of the modified V2PM and the corresponding calibration and compensation approaches, Section III describes the experimental setup and protocol, Section IV describes the experimental results, and, finally, Section V concludes the paper.

II. Principle and Method

To realize large-scale interferometric measurement, a photonic integrated interferometer array with the "pairwise static ABCD" scheme is used for multi-channel beam combination, which is basically a Michelson-type configuration [27], [28]. Furthermore, the arrayed waveguide gratings can be integrated with the interferometers to realize wide-band and multi-spectral interferometric measurement [29], [30]. With the switches and delay-lines built in the fiber channels, the beam combiner can be calibrated using the calibration source. A schematic layout of the photonic integrated interferometric imaging system is shown in Fig. 1.

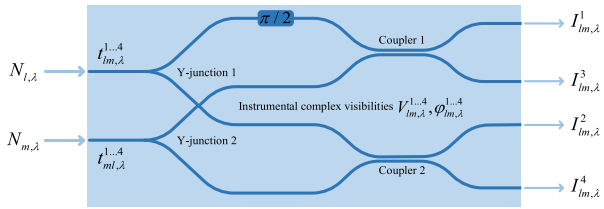

Fig. 2. Instrumental model of the photonic integrated interferometer.

The photonic integrated beam combiner can be regarded as an array of independent and identical interferometers, where each unit realizes the same function of narrow-band two-channel beam combination. The beam combing unit can be represented with the instrumental model, as shown in Fig. 2, where l and m denote the indices of input channels, $k = [1, 2, 3, 4]$ denote the indexes of output channels, λ denotes the spectral bands of beam combination, $N_{l,\lambda}$ and $N_{m,\lambda}$ denote the input intensities, $I^k_{lm,\lambda}$ denote the output intensities, $t^k_{lm,\lambda}$ and $t^k_{ml,\lambda}$ denote the instrumental transmittances, and $V^k_{lm,\lambda}$ and $\varphi^k_{lm,\lambda}$ denote the amplitudes and phases of instrumental visibilities.

Based on the above instrumental model, the photonic integrated interferometric measurement can be expressed as [24]

$$\begin{aligned} I^k_{lm,\lambda} &= N_{l,\lambda} t^k_{lm,\lambda} + N_{m,\lambda} t^k_{ml,\lambda} \\ &\quad + 2V^{obj}_{lm,\lambda} V^k_{lm,\lambda} \sqrt{N_{l,\lambda} t^k_{lm,\lambda} N_{m,\lambda} t^k_{ml,\lambda}} \\ &\quad \cos\left(\varphi^{obj}_{lm,\lambda} + \varphi^p_{lm,\lambda} + \varphi^k_{lm,\lambda}\right) \end{aligned} \tag{1}$$

where $V^{obj}_{lm,\lambda}$ and $\varphi^{obj}_{lm,\lambda}$ denote the amplitudes and phases of object visibilities and $\varphi^p_{lm,\lambda}$ denote the OPDs between the interferometric channels.

The modified V2PM used to express the relationship between the instrumental output intensities, amplitudes, and phases of object visibilities is represented as

$$V2PM = \begin{bmatrix} t^1_{lm,\lambda} & t^1_{ml,\lambda} & X^1_{lm,\lambda} & Y^1_{lm,\lambda} \\ t^2_{lm,\lambda} & t^2_{ml,\lambda} & X^2_{lm,\lambda} & Y^2_{lm,\lambda} \\ t^3_{lm,\lambda} & t^3_{ml,\lambda} & X^3_{lm,\lambda} & Y^3_{lm,\lambda} \\ t^4_{lm,\lambda} & t^4_{ml,\lambda} & X^4_{lm,\lambda} & Y^4_{lm,\lambda} \end{bmatrix},$$

$$\begin{aligned} X^k_{lm,\lambda} &= 2V^k_{lm,\lambda} \sqrt{t^k_{lm,\lambda} t^k_{ml,\lambda}} \cos\varphi^k_{lm,\lambda} \\ Y^k_{lm,\lambda} &= -2V^k_{lm,\lambda} \sqrt{t^k_{lm,\lambda} t^k_{ml,\lambda}} \sin\varphi^k_{lm,\lambda} \end{aligned} \tag{2}$$

where $X^k_{lm,\lambda}$ and $Y^k_{lm,\lambda}$ correspond to the level at which the beam combiner conserves coherence of light. With the modified V2PM, (1) can be represented as

$$\begin{bmatrix} I^1_{lm,\lambda} \\ I^2_{lm,\lambda} \\ I^3_{lm,\lambda} \\ I^4_{lm,\lambda} \end{bmatrix} = V2PM \cdot \begin{bmatrix} N_{l,\lambda} \\ N_{m,\lambda} \\ \sqrt{N_{l,\lambda} N_{m,\lambda}} X^{obj}_{lm,\lambda} \\ \sqrt{N_{l,\lambda} N_{m,\lambda}} Y^{obj}_{lm,\lambda} \end{bmatrix},$$

TABLE I
CALIBRATION PROCEDURE AND ESTIMATION METHOD WITH MODIFIED V2PM

Steps	Calibration procedure	Estimation method
Step1: $t^k_{lm,\lambda}$	Set input $N_{l,\lambda}=N^0_{l,\lambda}$ (fixed value), and $N_{m,\lambda}=0$ (switched off). Measure output $I^k_{lm,\lambda}(1)$.	$t^k_{lm\lambda}=\frac{I^k_{lm,\lambda}(1)}{N^0_{l,\lambda}}$, where $N^0_{l,\lambda}=\sum_{k=1}^{4} I^k_{lm,\lambda}(1)$.
Step2: $t^k_{ml,\lambda}$	Set input $N_{l,\lambda}=0$ (switched off), and $N_{m,\lambda}=N^0_{m,\lambda}$ (fixed value). Measure output $I^k_{lm,\lambda}(2)$.	$t^k_{ml,\lambda}=\frac{I^k_{lm,\lambda}(2)}{N^0_{m,\lambda}}$, where $N^0_{m,\lambda}=\sum_{k=1}^{4} I^k_{lm,\lambda}(2)$.
Step3: $X^k_{lm,\lambda}$	Set input $N_{l,\lambda}=N^0_{l,\lambda}$ (fixed value), $N_{m,\lambda}=N^0_{m,\lambda}$ (fixed value), and $\varphi^p_{lm,\lambda}=0$ (zero OPD). Measure output $I^k_{lm,\lambda}(3)$.	$X^k_{ml,\lambda}=\frac{I^k_{lm,\lambda}(3)-N^0_{l,\lambda}t^k_{lm,\lambda}-N^0_{m,\lambda}t^k_{ml,\lambda}}{\sqrt{N^0_{l,\lambda}N^0_{m,\lambda}}}$
Step4: $Y^k_{lm,\lambda}$	Set input $N_{l,\lambda}=N^0_{l,\lambda}$ (fixed value), $N_{m,\lambda}=N^0_{m,\lambda}$ (fixed value), and $\varphi^p_{lm,\lambda}=\pm\pi/2$ ($\pm\lambda/4$ OPD). Measure output $I^k_{lm,\lambda}(4)$.	$Y^k_{ml,\lambda}=\pm\frac{I^k_{lm,\lambda}(4)-N^0_{l,\lambda}t^k_{lm,\lambda}-N^0_{m,\lambda}t^k_{ml,\lambda}}{\sqrt{N^0_{l,\lambda}N^0_{m,\lambda}}}$

$$\begin{aligned} X^{obj}_{lm,\lambda} &= V^{obj}_{lm,\lambda}\cos\left(\varphi^{obj}_{lm,\lambda}+\varphi^{p}_{lm,\lambda}\right) \\ Y^{obj}_{lm,\lambda} &= V^{obj}_{lm,\lambda}\sin\left(\varphi^{obj}_{lm,\lambda}+\varphi^{p}_{lm,\lambda}\right) \end{aligned} \tag{3}$$

To construct the modified V2PM, a monochrome point source is used as the object ($V^{obj}_{lm,\lambda}=1$ and $\varphi^{obj}_{lm,\lambda}=0$). Then, the calibration procedure and estimation method can be divided into four steps, as shown in Table I. Here, Steps 1–2 realize the photometric calibration, and Steps 3–4 realize the interferometric calibration.

With the calibration data, the amplitudes and phases of instrumental visibilities can be derived as

$$\begin{aligned} V^{k}_{lm,\lambda} &= \frac{\sqrt{\left(X^k_{lm,\lambda}\right)^2+\left(Y^k_{lm,\lambda}\right)^2}}{2\sqrt{t^k_{lm,\lambda}t^k_{ml,\lambda}}}, \\ \varphi^{k}_{lm,\lambda} &= -\tan^{-1}\left(Y^k_{lm,\lambda}/X^k_{lm,\lambda}\right) \end{aligned} \tag{4}$$

The pixel to visibility matrix (P2VM), which is used to compensate the instrumental errors, can be derived via an inverse operation on the V2PM equation as

$$\begin{bmatrix} N_{l,\lambda} \\ N_{m,\lambda} \\ \sqrt{N_{l,\lambda}N_{m,\lambda}}X^{obj}_{lm,\lambda} \\ \sqrt{N_{l,\lambda}N_{m,\lambda}}Y^{obj}_{lm,\lambda} \end{bmatrix} = P2VM\cdot\begin{bmatrix} I^1_{lm,\lambda} \\ I^2_{lm,\lambda} \\ I^3_{lm,\lambda} \\ I^4_{lm,\lambda} \end{bmatrix},$$

TABLE II
COMPARISON BETWEEN CONVENTIONAL V2PM AND MODIFIED V2PM

Conventional V2PM	$\begin{bmatrix} t^1_{lm,\lambda} & t^1_{ml,\lambda} & V^1_{lm,\lambda}*X^1_{lm,\lambda} \\ t^2_{lm,\lambda} & t^2_{ml,\lambda} & V^2_{lm,\lambda}*X^2_{lm,\lambda} \\ t^3_{lm,\lambda} & t^3_{ml,\lambda} & V^3_{lm,\lambda}*X^3_{lm,\lambda} \\ t^4_{lm,\lambda} & t^4_{ml,\lambda} & V^4_{lm,\lambda}*X^4_{lm,\lambda} \end{bmatrix}$
Modified V2PM	$\begin{bmatrix} t^1_{lm,\lambda} & t^1_{ml,\lambda} & X^1_{lm,\lambda} & Y^1_{lm,\lambda} \\ t^2_{lm,\lambda} & t^2_{ml,\lambda} & X^2_{lm,\lambda} & Y^2_{lm,\lambda} \\ t^3_{lm,\lambda} & t^3_{ml,\lambda} & X^3_{lm,\lambda} & Y^3_{lm,\lambda} \\ t^4_{lm,\lambda} & t^4_{ml,\lambda} & X^4_{lm,\lambda} & Y^4_{lm,\lambda} \end{bmatrix}$

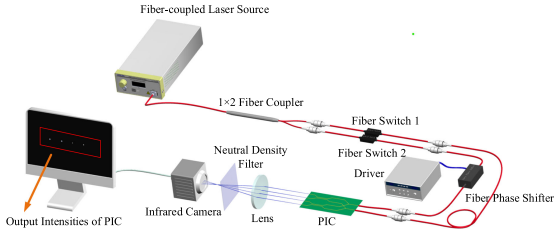

Fig. 3. Schematic model of the photonic integrated interferometer.

$$\begin{aligned} V^{obj}_{lm,\lambda} &= \sqrt{\left(X^{obj}_{lm,\lambda}\right)^2+\left(Y^{obj}_{lm,\lambda}\right)^2} \\ \varphi^{obj}_{lm,\lambda}+\varphi^{p}_{lm,\lambda} &= \tan^{-1}\left(Y^{obj}_{lm,\lambda}\Big/X^{obj}_{lm,\lambda}\right) \end{aligned} \tag{5}$$

To realize high-accuracy interferometric measurement of object visibilities, OPD $\varphi^p_{lm,\lambda}$ should be reduced as much as possible and kept stable by fringe tracking. However, this discussion is beyond the scope of this paper. In the following sections, it is assumed that $\varphi^p_{lm,\lambda}$ can be finely controlled, without any influence on the measurement.

Table II shows the comparison between conventional and modified V2PMs. These two V2PMs are mathematical transformations of (1), and the different forms of V2PM correspond to the different calibration strategies. The photometric calibration procedure is the same for both V2PM estimators. For interferometric calibration of conventional V2PM, instrumental visibilities are derived from interferograms, which can be obtained with temporal modulation of $\varphi^p_{lm,\lambda}$. During calibration, $\varphi^p_{lm,\lambda}$ must be adjusted continuously to achieve fitting of interferogram. In the calibration procedure of the modified V2PM, the value of $\varphi^p_{lm,\lambda}$only requires a single adjustment to achieve the calibration of $X^k_{ml,\lambda}$ and $Y^k_{ml,\lambda}$. The instrumental visibilities can be obtained using (4). The calibration approach based on the modified V2PM greatly simplifies the calibration procedure, and high-accuracy measurements of interferometric visibilities can be realized efficiently.

III. EXPERIMENTAL SETUP

Fig. 3 shows the constructed experimental setup to validate the proposed approach, where a custom-mode two-channel silica-based interferometric PIC is used for beam combination in the narrow-band of 1550 nm. A fiber-coupled laser source (Thorlabs S1FC1550PM) is used as the calibration source, and

TABLE III
EXPERIMENTAL PROTOCOL OF FOUR-STEP CALIBRATIONS

Steps	Phase shift (driving voltage)	Optical Switch 1	Optical Switch 2
Step 1	Referenced 0 (300 mV)	On	Off
Step 2	Referenced 0 (300 mV)	Off	On
Step 3	Referenced 0 (300 mV)	On	On
Step 4	Referenced $\pi/2$ (350 mV) Referenced $-\pi/2$ (250 mV)	On	On

TABLE IV
ESTIMATED PARAMETERS OF MODIFIED V2PM WITH FOUR-STEP CALIBRATION

k	t_{12}	t_{21}	X_{12}	$Y_{12}(+\pi/2)$	$Y_{12}(-\pi/2)$
1	0.252	0.243	-0.443	0.021	-0.027
2	0.250	0.245	0.005	-0.436	-0.469
3	0.256	0.258	0.480	-0.009	-0.002
4	0.242	0.254	0.000	0.481	0.434

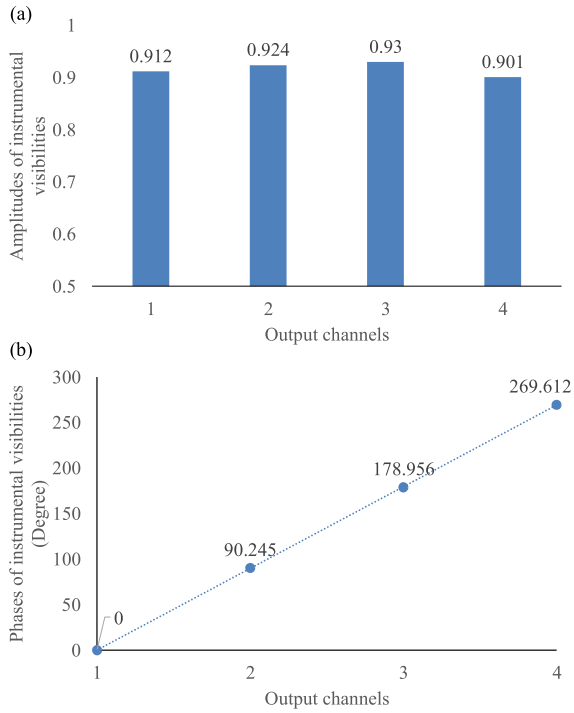

Fig. 4. Amplitudes and phases (considering the phase of channel 1 as the reference) of instrumental visibilities.

its output beam is divided into two components with a 1×2 single-mode fiber coupler. For each interferometric channel, the switching condition is controlled by a fiber optical switch (Thorlabs SOA1013SXS). In the optical path of one channel, a fiber phase shifter (General Photonics FPS-002) is used for the fine tuning of OPDs with a dynamic range of 65π and tuning precision of 0.1π, and th e driver (General Photonics MPD-001) has a closed loop gain of 30 V/V. In the corresponding optical path of the other channel, an equal-length single-mode fiber is used to compensate for the OPD between the two channels. The output beams of the PIC are imaged with an infrared camera (LeadingOE LD-SW6401715-C) through a lens of 30-mm focal length, and a 1% neutral density filter is inserted to decrease the output intensities of the PIC.

In the calibration procedure, the driving frequency of the phase shifter is set to 500 Hz, where a 200 mV change in the driving voltage corresponds to a 2π phase shift. The initial driving voltage is set to 300 mV as the reference zero to ensure that the phase shifter operates in the linear range. The infrared camera is thermoelectrically cooled to reduce the background and readout noise, and the exposure time is set to 25 μs. Table III presents the experimental protocol of the four-step calibrations.

In each calibration step, the blob image captured by the infrared camera is filtered with an appropriate grayscale threshold. Then, four blobs of PIC output are extracted, and the corresponding cumulative grayscales are calculated. Finally, the grayscales of the four blobs are normalized as the PIC output intensities, which are used to estimate the modified V2PM of the photonic integrated beam combiner.

IV. RESULTS AND DISCUSSIONS

Table IV presents the estimated parameters of the modified V2PM with four-step calibration obtained via a 100-fold statistical average of the measurement results. Compared to the conventional approach [31], the standard deviation of the normalized transmittances is less than 2.43%, which has little influence on the measurement accuracy of interferometric visibilities. However, there are noticeable differences between the measurement results at $\pm\pi/2$ phase shifts, which may be induced mainly by the hysteresis effect of piezoelectric actuators in the phase shifters. To improve the measurement accuracy of phase shifting, we used the average values at $\pm\pi/2$ phase shifts as the estimated items in the modified V2PM.

Ideally, the light energy coupled into PIC is uniformly distributed into four channels during photometric calibration, and the values of t_{12}^k and t_{21}^k are the same. However, this is limited by the semiconductor manufacturing process. The Y-junctions and couplers in PIC do not present a perfect splitting ratio, and crosstalk and loss of cross waveguides are unavoidable. These factors lead to different transmission characteristics of each channel, which are reflected in the measured value of t_{12}^k and t_{21}^k. The instrumental visibility can also be affected as the difference in transmission characteristics, resulting in X_{12}^k and Y_{12}^k deviating from the theoretical value.

The instrumental visibilities derived from the calibration data of the modified V2PM are shown in Fig. 4 . All amplitudes of instrumental visibilities are larger than 0.9, and the deviations are less than 2.9%. The deviation of the referenced phases of instrumental visibilities is less than 1.41% of that in the conventional approach [31], which confirms that the proposed approach can calibrate the instrumental characterization accurately.

To validate the compensation capabilities with the calibrated V2PM, we reused the calibration source as the object and

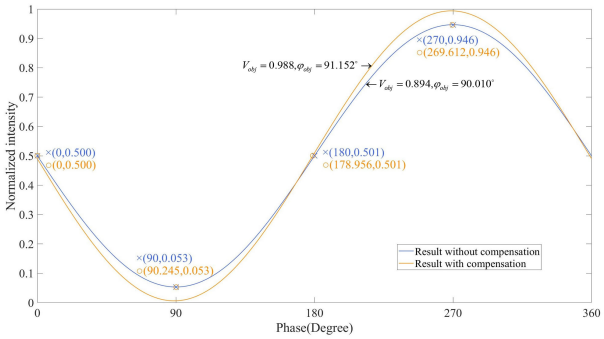

Fig. 5. Comparison of fitted interferometric patterns between the direct and compensated estimations.

change the settings of the optical intensities and channel OPDs randomly. As shown in Fig. 5, the fitted interferometric patterns of measurement results are compared between the direct and compensated estimations. After compensation with P2VM, it can be observed that the amplitude of the object visibility is improved from 0.894 to 0.988, which confirms the calibration accuracy of the proposed approach, as the compensated results are close to the assumptions of the object source. It is also evident that the fitted interferometric patterns are rather sensitive to the phase relations between the output channels, which proves that the phase accuracy during beam combiner calibration is more important for realizing high-accuracy interferometric measurement.

The experimental results validate the efficiency and high-accuracy of the proposed approach for beam combiner calibration, which can be easily extended and automated for large-scale photonic integrated interferometric measurements. With the capabilities of online calibration and compensation, the environmental influences on interferometric measurement can be minimized, which is critical for optical synthetic aperture systems, especially for operation in harsh environments such as space-borne and air-borne applications.

REFERENCES

[1] J. Bland-Hawthorn and P. Kern, "Astrophotonics: A new era for astronomical instruments," *Opt. Exp.*, vol. 17, pp. 1880–1884, Mar. 2009, doi: 10.1364/OE.17.001880.

[2] L. Labadie *et al.*, "Astronomical photonics in the context of infrared interferometry and high-resolution spectroscopy," in *Proc. SPIE Astronomical Telescopes + Instrum. Conf.*, Edinburgh, U.K., Jun. 2016, Art. no. 990718.

[3] J. Bland-Hawthorn and S. Leon-Saval, "Astrophotonics: Molding the flow of light in astronomical instruments," *Opt. Exp.,* vol. 25, pp. 15549–15557, Jun. 2017, doi: 10.1364/OE.25.015549.

[4] R. P. Scott *et al.*, "Demonstration of a photonic integrated circuit for multi-baseline interferometric imaging," in *Proc. IEEE Photon. Conf.*, San Diego, CA, USA, 2014, pp. 1–2.

[5] F. Malbet, P. Kern, I. Schanen-Duport, J. Berger, and K. Perraut, "Integrated optics for astronomical interferometry. I. Concept and astronomical applications," *Astron. Astrophys. Suppl. Ser.*, vol. 138, pp. 135–145, Feb. 1999, doi: 10.1051/aas:1999496.

[6] P. Kervella, V. Foresto, A. Glindemann, and R. Hofmann, "VINCI: The VLT interferometer commissioning instrument," in *Proc. SPIE - Int. Soc. for Opt. Eng.*, Munich, Germany, Jul. 2000,pp.31–42.

[7] J.-P. Berger *et al.*, "An integrated-optics 3-way beam combiner for IOTA," in *Proc. SPIE - Int. Soc. for Opt. Eng.*, HI, United States, Feb. 2003, Art. no. 8.

[8] R. Abuter *et al.*, "First light for GRAVITY: Phase referencing optical interferometry for the very large telescope interferometer," *Astron. Astrophys.*, vol. 602, p. A94, May 2017, doi: 10.1051/0004-6361/201730838.

[9] R. L. Kendrick, A. Duncan, C. Ogden, J. Wilm, and S. T. Thurman, "Segmented planar imaging detector for EO reconnaissance," in *Proc. OSA Tech. Dig.*, Jun. 2013, Art. no. CM4C.1.

[10] R. L. Kendrick *et al.*, "Flat-panel space-based space surveillance sensor," in *Proc. Int. Conf. Adv. Maui Opt. Space Surveill. Technol. Conf.*, Sep. 2013, pp. 1–9.

[11] A. Duncan *et al.*, "Spider: Next generation chip scale imaging sensor," in *Proc. Int. Conf. Maui Opt. Space Surveill. Technol. Conf.*, 2015, pp. 1–9.

[12] W. Gao, Y. Yuan, X. Wang, L. Ma, Z. Zhao, and H. Yuan, "Quantitative analysis and optimization design of the segmented planar integrated optical imaging system based on an inhomogeneous multistage sampling lens array," *Opt. Exp.*, vol. 29, no. 8, pp. 11869–11884, 2021.

[13] H. Hu, C. Liu, Y. Zhang, Q. Feng, and S. Liu, "Optimal design of segmented planar imaging for dense azimuthal sampling lens array," *Opt. Exp.*, vol. 29, no. 15, pp. 24300–24314, 2021.

[14] K. Badham *et al.*, "Photonic integrated circuit-based imaging system for SPIDER," in *Proc. Conf. Lasers Electro-Opt. Pacific Rim*, Singapore, Jul. 2017, pp. 1–5.

[15] T. Su *et al.*, "Interferometric imaging using Si3N4 photonic integrated circuits for a SPIDER imager," *Opt. Exp.*, vol. 26, no. 10, pp. 12801–12812, May 2018, doi: 10.1364/OE.26.012801.

[16] P. Gatkine *et al.*, Astro2020: Astrophotonics White Paper, Jul. 2019, *arXiv:1907.05904*.

[17] J. Allington-Smith *et al.*, "Defining requirements and identifying relevant technologies in astrophotonics," in *Proc. SPIE - Int. Soc. Opt. Eng.*, Jul. 2010, Art. no. 773925.

[18] T. Chen *et al.*, "Sparse-aperture photonics-integrated interferometer (SPIN) imaging system: Structural design and imaging quality analysis," *Opt. Exp.*, vol. 29, no. 24, pp. 39256–39270, 2021.

[19] J. W. Goodman and L. M. Narducci, "Statistical optics," *Phys. Today*, vol. 39, no. 10, pp. 126–126, 1986.

[20] M. Shao and D. Staelin, "Long-baseline optical interferometer for astrometry," *J. Opt. Soc. Amer. (1917-1983)*, vol. 67, pp. 81–86, Jan, 1977, doi: 10.1364/JOSA.67.000081.

[21] T. Su *et al.*, "Experimental demonstration of interferometric imaging using photonic integrated circuits," *Opt. Exp.*, vol. 25, no. 11, pp. 12653–12665, May 2017, doi: 10.1364/OE.25.012653.

[22] Z. Fang, K. Chin, R. Qu, and H. Cai, "Fundamentals of optical fiber sensors," *Phys. Today*, vol. 49, no. 2, pp. 10–75, 2012.

[23] S. Lacour *et al.*, "Characterization of integrated optics components for the second generation of VLTI instruments," in *Proc. SPIE Astronomical Telescopes + Instrum. Conf.*, Marseille, France, Aug. 2008, vol. 7013, doi: 10.1117/12.789795.

[24] M. Benisty *et al.*, "An integrated optics beam combiner for the second generation VLTI instruments," *Astron. Astrophys.,* vol. 498, pp. 601–613, Mar. 2009.

[25] M. Creech-Eakman *et al.*, "The magdalena ridge observatory interferometer: 2014 status update," in *Proc. SPIE - Int. Soc. Opt. Eng.*, Jul. 2012, vol. 9146, doi: 10.1117/12.2057331.

[26] A. Glindemann, *Principles of Stellar Interferometry*. Berlin, Germany: Springer, 2011.

[27] W. Gao, X. Wang, L. Ma, Y. Yuan, and D. Guo, "Quantitative analysis of segmented planar imaging quality based on hierarchical multistage sampling lens array," *Opt. Exp.*, vol. 27, pp. 7955–7967, Mar. 2019, doi: 10.1364/OE.27.007955.

[28] A. Thompson, J. Moran, and J. G. Swenson, *Interferometry and Synthesis in Radio Astronomy*, 2nd ed., Berlin, Germany: Springer May 2001.

[29] Z. Zhang *et al.*, "Low-crosstalk silicon photonics arrayed waveguide grating," *Chin. Opt. Lett.,* vol. 15, Apr. 2017, pp. 041301–041304, doi: 10.3788/COL2017-15.041301.

[30] G. Liu, D. Wen, Z. Song, and T. Jiang, "System design of an optical interferometer based on compressive sensing: An update," *Opt. Exp.*, vol. 28, no. 13, pp. 19349–19361, 2020.

[31] H. Chen, "Design and optimization of the silica-based 90 degree optical hybrid," (in Chinese), M.S. thesis, Dept. Elect. Eng., Zhejiang Univ., HangZhou, China, 2019. [Online]. Available: https://kns.cnki.net/KCMS/detail/detail.aspx?dbcode=CMFD&filename=1019034511.nh